# X-ray diffraction study of damage induced by swift heavy ion irradiation in fluorapatite

S. Miro [a], D. Grebille [a], D. Chateigner [a], D. Pelloquin [a], J.-P. Stoquert [c],
J.-J. Grob [c], J.-M. Costantini [b], F. Studer [a,*]

[a] *CRISMAT (CNRS UMR 6508), ENSICAEN, 6, Bd du Marechal Juin, F-14050 Caen cedex, France*
[b] *CEA-SACLAY, DMN/SRMA, F-91191 Gif-sur-Yvette Cedex, France*
[c] *Laboratoire PHASE-23, rue du Loess, BP 20 CR, F-67037 Strasbourg cedex 2, France*

## Abstract

X-ray powder and high-resolution single-crystal diffraction techniques were used to study the irradiation damage of fluorapatites. Krypton, iodine and carbon irradiations were performed at high energy ($\approx 1\,\mathrm{MeV/a}$) in the $10^{11}$ to $5 \times 10^{13}\,\mathrm{cm}^{-2}$ fluence range. Both diffraction techniques showed a strong unit-cell increase of the fluorapatite structure, with a full relaxation of the remaining part of the material for large fluences. X-ray powder experiments revealed an amorphization of the material up to 85% for fluences around $10^{13}$ ions cm$^{-2}$. Simulation of the relationship between amorphous volume fraction and fluence evidenced that the amorphization mechanisms could be dominated by a single impact process for iodine and double impacts for krypton. The effective radius of the track core remained nearly constant although the electronic energy loss increases from Kr to I. Moreover total amorphization of fluorapatite irradiated by swift heavy ions could not be obtained in this study. Experiments performed on (0 0 2)-oriented single-crystals allowed us to separate the change of the $c$-parameters of the damaged and virgin phases, and pointed out an anisotropic response of the material to the damage process.
© 2004 Elsevier B.V. All rights reserved.

PACS: 61.80.jh
Keywords: Swift heavy ion; Irradiation damage; Apatite; Nuclear waste; Irradiation induced stress

## 1. Introduction

Since the beginning of the nuclear power plant era, the storage of nuclear waste over geological periods is one of the main problems that have to

be addressed by the nuclear industry. Dealing with the problems of nuclear waste storage, the synthesis of new specific storage matrices and the study of their sensitivity to irradiation (γ-rays, α particles, fission fragments) was strongly supported by the governmental administration and thus was the object of many studies. Among the studied matrices, apatites were considered rather early since their structure allow them to incorporate many elements such as I, Cs and/or trivalent actinides [1–5]. Apatite, in its most common high-symmetry representation [6], is the generic name of a family of calcium phosphates with formula $Me_{10}(XO_4)_6Y_2$ which crystallize in the hexagonal system of space group $P6_3/m$. The Me atoms stand for divalent cations (Ca, Ba, Pb) suitable for substitution by monovalent (Na, Rb, Cs) or trivalent (Al, Nd, La) cations, while the $XO_4$ group is a trivalent anion ($PO_4^{2-}$, $VO_4^{3-}$) able to be substituted by tetravalent or divalent groups ($SiO_4^{4-}$, $GeO_4^{4-}$ or $SO_4^{2-}$, $CO_3^{2-}$, $HPO_4^{2-}$, respectively). The charge is balanced by monovalent anions Y such as $F^-$ (fluorapatite), $Cl^-$ (chlorapatite), $OH^-$ (hydroxyapatite) [7–9]. The apatitic structure is built up of a frame of $XO_4^{3-}$ groups giving rise to two types of tunnels. The first tunnel type is made of Me(I) atoms with four Me cations in the (4f) sites of the structure surrounded by nine oxygen atoms, whereas the second tunnel type is formed of six Me(II) cations in the (6h) sites surrounded by six oxygen atoms and one Y atoms.
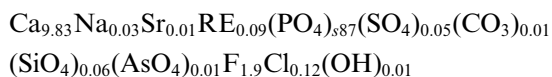
The flexibility of the apatitic structure versus substitution explains why the silicate substituted apatites also known as britholites, can be used to store iodine, cesium and minor trivalent actinides. Apatites also exhibit a high chemical stability in slightly alkaline water medium and are stable against radioactive excitations: some natural apatites found in In-Ouzzal (Algeria) maintained their crystallized structure (non metamict) despite their irradiation to a fluence two to three times higher than the amorphization dose. Furthermore, apatite being the thermodynamically stable form of calcium phosphate, is one of the most abundant natural minerals on the earth surface. The most common apatites are the fluor- and hydroxyapatites of respective formula $Ca_{10}(PO_4)_6F_2$ and $Ca_{10}(PO_4)_6(OH)_2$.

Nuclear waste are mainly composed of actinides produced by nuclear transmutation inside reactors (Np, Pu, Am, Cu) and by fission products (Sr, I, Gd, Cs) resulting from the fission of $^{235}U$. After their production, most of these radionuclides transform following a complex scheme of spontaneous disintegrations characterized by the emission of α particles. In this way, the damage is mainly due to cascades of nuclear collisions created by the corresponding nuclei recoils [10–12]. Spontaneous fission, which occurs only for a few elements (Np, U, Pu), is less probable but results in the production of highly energetic ions (up to 100 MeV) with masses around 100. Thus, during long time storage of nuclear wastes, the matrices can be damaged either by α particles and heavy atoms in the nuclear collision regime or by energetic lighter atoms produced by the fission process in the electronic energy loss regime.

In this paper, we focus on fluorapatites irradiated by heavy ions (Kr, I) in order to simulate the damage induced by fission fragments and with C ions for α recoils (in the nuclear stopping region). We used X-ray diffraction on natural single crystals and synthetic sinters to investigate the damage and the correlated stress produced in the thin irradiated layer of the samples.

## 2. Experimental

Fluorapatite sinters with formula $Ca_{10}(PO_4)_6F_2$ were synthesized by direct solid state reaction between $CaF_2$, CaO, $Ca_2P_2O_7$ and $CaHPO_4$ chemicals. After thorough mixing, powder is pressed into disks and heated at 1500 °C during 6h in nitrogen flux [1,2]. The studied single crystals are natural minerals coming from Durango (Mexico) with chemical composition:

$Ca_{9.83}Na_{0.03}Sr_{0.01}RE_{0.09}(PO_4)_{s87}(SO_4)_{0.05}(CO_3)_{0.01}$
$(SiO_4)_{0.06}(AsO_4)_{0.01}F_{1.9}Cl_{0.12}(OH)_{0.01}$

(RE: rare earths) measured by Young et al. [13]. Single crystals were cut and irradiated perpendicularly to the *c*-axis. Crystals and sintered disks were then polished and annealed at 500 °C in air during

Table 1
Irradiation parameters in fluorapatites for the three heavy ions used in this study

| Ion | $^{12}C$ | $^{86}Kr^{21+}$ | $^{127}I^{10+}$ |
|---|---|---|---|
| Energy (MeV) | 12 | 70 | 120 |
| $R_p$ (μm) | 7.7 | 9.4 | 12.7 |
| $\Delta R_p$ (μm) | 0.23 | 0.33 | 0.48 |
| $\langle (dE/dx)_e \rangle$ (keV/nm) | 1.6 | 12.7 | 18.7 |
| $\langle (dE/dx)_n \rangle$ (keV/nm) | $1.5 \times 10^{-3}$ | $5.4 \times 10^{-3}$ | $9.3 \times 10^{-3}$ |

6 h to relax strains and contaminants desorbed from the surface solvent.

Samples were irradiated at a constant temperature of 10 °C with $^{12}C$ and $^{87}Kr$ ions delivered by the IRRSUD beamline of the GANIL facility (Caen, France). Total energy was set to 12 MeV and 70 MeV for C and Kr ions, respectively. The irradiation with Iodine was performed at room temperature at a total energy of 120 MeV using the Vivitron facility (Strasbourg, France). Kr and I irradiations were used to simulate fission fragments of respectively low and high mass at fluences ranging from $10^{11}$ to $5 \times 10^{13}$ cm$^{-2}$ (Table 1). The carbon irradiation was used to simulate α recoils in the nuclear energy loss regime far below the damage threshold due to electronic energy loss.

Powder X-ray diffraction was operated on a 4-circle diffractometer equipped with a curved position sensitive detector (INEL CPS 120), using the copper Kα radiation [14]. The use of the CPS enables the acquisition of the full diagram within $0° \leqslant 2\theta \leqslant 120°$ range in one step. The incidence angle of the X-ray beam was 5° relative to the sample plane in order to probe the near surface of the sintered pellets. Under this condition, 97% of the diffracted signal comes from the first 9 μm of the sample, which corresponds to the estimated thickness modified by Kr ions. In order to minimise texture effects on the diffraction patterns, the samples were rotated around an axis normal to their surface during acquisition. However, texture could not be fully removed using only this rotation, and more rotations could not be operated because of too small sample sizes. Collimating slits of 200 μm were used in order to decrease as much as possible the instrumental contributions to the peak broadening. After deconvolution of the instrumental broadening measured on the

SRM 660 LaB$_6$ standard powder from NIST [15], the mean crystallite sizes was determined using the Rietveld approach. In order to quantitatively determine the amorphized volumic fraction of the perturbed layer, a quantitative phase analysis was operated through the X-ray combined approach [16], taking account of an arbitrary texture of the remaining crystalline part of the layer. The measured crystalline phase corresponds to fluorapatite with various crystallite sizes and unit-cell dimensions depending on the irradiation conditions. The amorphous phase was modelled using the fluorapatite structure with elongated cell parameters and very small crystal sizes, typically from 40 Å to smaller than the crystal unit-cell. All the refinements were operated using the software package MAUD [17,18]. Counting times of around 24 h were necessary to detect amorphous fractions below 5% in volume.

High resolution single crystal X-ray diffraction experiments were performed on a Philips MRD diffractometer using the monochromatized Cu-Kα1 line. A parallel beam with a 25 s of arc divergence is produced by a focussing hybrid mirror and a Ge-220 monochromator. A high resolution signal is obtained using a channel cut Ge-220 analyser. Single crystal samples were oriented using a Eulerian cradle with the hexagonal axis in the bisecting position in the diffraction plane. According to the crystal morphology and to the irradiation direction, it was not possible in this symmetrical configuration to change the incidence angle and consequently the X-ray beam probed both irradiated and virgin parts of the sample. The beam incidence was swept around 13° with respect to the normal to the crystal surface for the [0 0 2] reflection presented in this work. As a consequence, 95% of the measured scattered signal comes from a superficial layer of 12 μm and the irradiated damaged layer (9 μm) is responsible for around 90% of the global scattering.

TEM analyses were carried out using a JEOL 2010 Cx microscope fitted with a eucentric goniometer (±60°) and equipped with an OXFORD-INCA analyser. Natural crystals and as ground samples were crushed in butanol and the small flakes were deposited on holey carbon grids before

irradiation by swift heavy ions. Only samples exposed to Kr ions were investigated.

## 3. Results and discussion

### 3.1. Fluorapatite sinters

The electron microscopy image (Fig. 1) of krypton irradiated fluorapatite microcrystals was taken with the electron beam parallel to the ion beam. The small white dots are ascribed to tracks created by the ions. The number of tracks ($1 \pm 0.05 \times 10^{11} \, cm^{-2}$) is in good agreement with the fluence ($10^{11} \, Kr \, cm^{-2}$) as estimated from the beam monitor. At this small fluence, no track overlapping occurs and each dot can be understood as a single ion impact. Beyond $10^{12} \, cm^{-2}$, track overlapping turns to be high enough to disturb the matrix analysis, especially the measure of the damage rate. Moreover the instability of fluorapatite under the electron beam, noticed by many authors in the past [11,17], prevented any longer observations at higher magnification to probe the amorphous nature of the track core. As shown earlier [26], the track is very likely not continuous but built up of bubbles of defects extending along the ion path. Nevertheless, from images such as the one shown in Fig. 1, a mean track diameter of 4 nm is obtained from the histogram of Fig. 1(b).

Powder X-ray diffraction was first carried out on sintered disks to measure the damaged fraction of the irradiated layer of thickness, $e_{irr}$, close to a calculated value of 9 μm. Figs. 2 and 3 show experimental data obtained for the virgin and highest Kr-irradiated fluence and for the least and highest I-irradiated fluences respectively; the X-ray refinement results for all the samples are presented in Table 2. Considering the complexity of the apatitic structure, a good agreement between experimental and calculated points can be observed for the pristine fluorapatite sample, with however relatively high reliability factors of $R_w = 26.9\%$ and $R_B = 15.8\%$ (Fig. 2(a)). The diagrams exhibit preferred $\{hk0\}$ reflections, as a sign of existence of a planar texture with $c$-axes of the hexagonal structure preferentially aligned parallel to the sample plane, with no preferred direction in this plane.
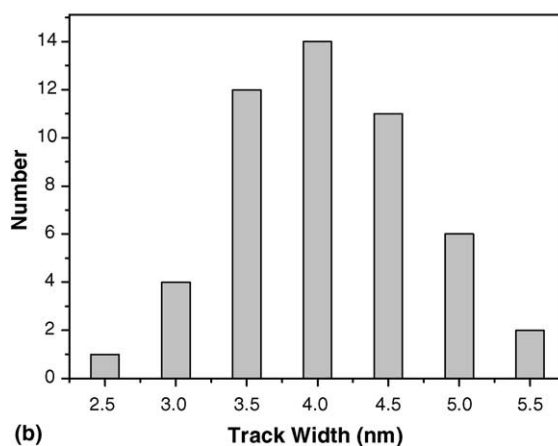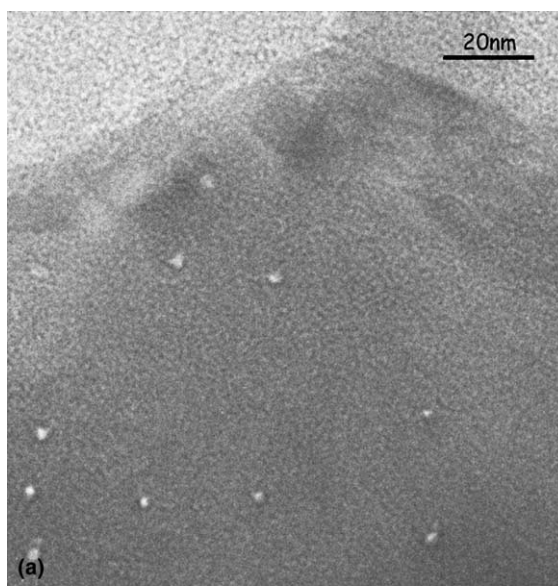


Fig. 1. (a) TEM micrograph of a fluorapatite crystal irradiated with 70 MeV Krypton ions with an estimated fluence of $(1 \pm 0.05) \times 10^{11} \, cm^{-2}$ ($\langle Se \rangle = 12.7 \, keV/nm$) and (b) corresponding histogram showing an average track diameter of 4 nm.

The texture is relatively smooth and all the peaks still appear in the diagrams (Fig. 2(a)), even those corresponding to the $c$-axes, and gives rise to an overall poor modelling of the diffractograms, and systematic deviations of the background at large $\theta$ values. This texture has to be corrected in the Rietveld approach in order to perform the best quantitative analysis, and particularly to determine volume fractions of the different phases.
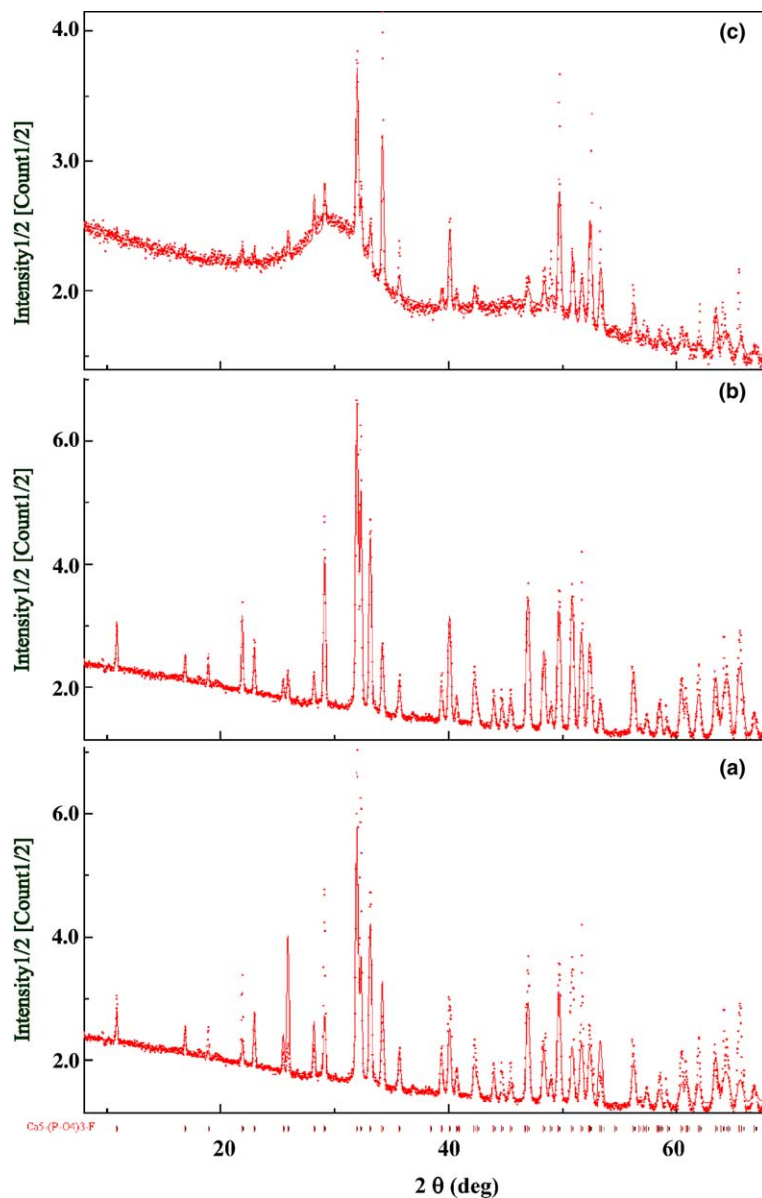
Fig. 2. Rietveld analysis examples: (a) non-irradiated sample without application of a texture correction, (b) with texture correction, (c) Kr-irradiated sample ($10^{13}$ cm$^{-2}$) with texture correction.

Fig. 2(b) illustrates a fit with texture correction for the sample of Fig. 2(a). The experimental points are significantly better reproduced with the texture correction, which decreases the reliability factors (Table 2). The described texture corresponds to our SEM observations showing needle-like grain

shapes with the needle axes aligned parallel to the sample plane.

In the case of Kr irradiation, for the lowest fluence ($10^{11}$ Kr cm$^{-2}$ and $10^{12}$ Kr cm$^{-2}$), no drastic change in the X-ray diagrams could be observed indicating that the fraction of disordered matter
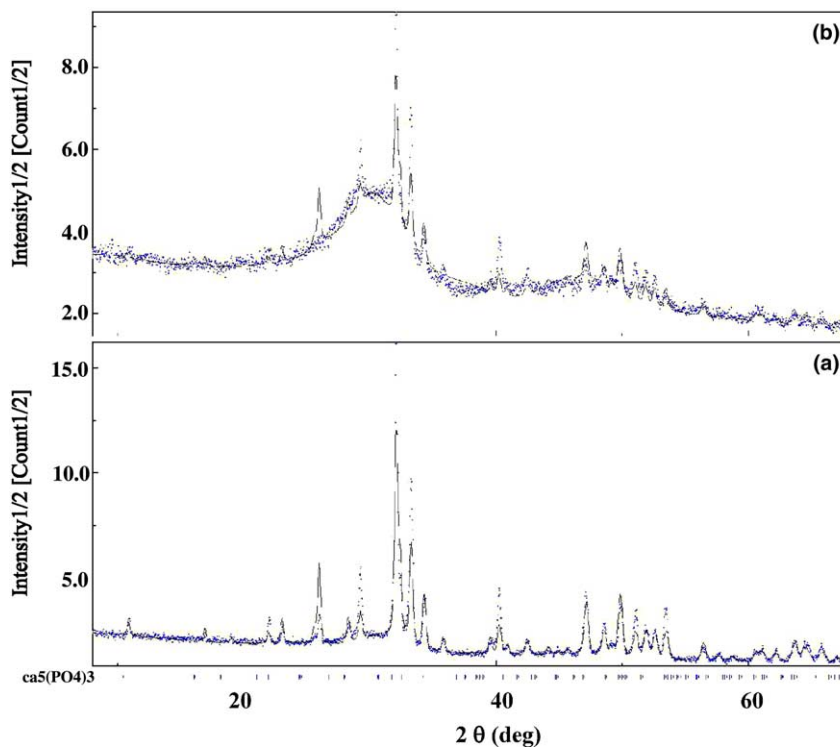
Fig. 3. Rietveld analysis of (a) the least ($5 \times 10^{11}$ cm$^{-2}$) and (b) most ($10^{13}$ cm$^{-2}$) I-irradiated samples, with texture correction.

Table 2
Parameter variations of fluoapatite sinters irradiated by Kr and I ions deduced from simulations of powder X-ray diffractograms with texture correction using the MAUD code [16,17]

| Fluence (ions cm$^{-2}$) | $V_c/V$ (%) | $a$ (Å) | $c$ (Å) | $\Delta a/a_0$ (%) | $\Delta c/c_0$ (%) | $R_w$ (%) | $R_B$ (%) |
|---|---|---|---|---|---|---|---|
| 0 | 100 | 9.3365(3) | 6.8560(5) | – | – | 14.3 | 8.7 |
| **Kr** | | | | | | | |
| $10^{11}$ | 100 | – | – | – | – | | |
| $10^{12}$ | 100 | – | – | – | – | | |
| $5 \times 10^{12}$ | 49(1) | 9.3775(9) | 6.8912(8) | 0.44 | 0.53 | 24 | 15 |
| $10^{13}$ | 20(1) | 9.4236(5) | 6.9105(5) | 0.94 | 0.82 | 9.9 | 6 |
| $5 \times 10^{13}$ | 14(1) | 9.3160(4) | 6.8402(5) | −0.21 | −0.22 | 10.5 | 5.9 |
| **I** | | | | | | | |
| $10^{11}$ | – | – | – | – | – | | |
| $5 \times 10^{11}$ | 86(2) | 9.3603(3) | 6.8790(5) | 0.26 | 0.35 | 23.9 | 15.1 |
| $10^{12}$ | 70(9) | 9.387(9) | 6.894(8) | 0.35 | 0.53 | 28.7 | 18 |
| $3 \times 10^{12}$ | 47(2) | 9.3645(3) | 6.8840(5) | 0.30 | 0.42 | 13.3 | 9 |
| $5 \times 10^{12}$ | 29.2(5) | 9.3765(5) | 6.8881(6) | 0.44 | 0.48 | 10.4 | 7.3 |
| $10^{13}$ | 13.2(2) | 9.3719(4) | 6.8857(6) | 0.38 | 0.45 | 6.7 | 4.9 |

remains smaller than 5%. However, no satisfactory cell parameters could be deduced because of peak shifts, probably due to the presence of residual strains in the powder. At such fluences elastic deformations are likely to exist; they are difficult to take into account in the fit because one would

have to determine residual stresses, cell parameters and texture from only one diagram. Conversely, as shown in Fig. 2(c), for a fluence of $10^{13}$ Kr cm$^{-2}$, diffractograms clearly exhibit a broad contribution centred on the most intense peaks of diffraction, corresponding to a growing fraction of disordered matter. This large peak is shifting continuously towards low $2\theta$ angles with increasing fluences, reaching $2\theta = 30°$ for $5 \times 10^{13}$ cm$^{-2}$. No change in the mean crystallite sizes ($\approx 300$ nm) occurs during irradiation, indicating that the non-amorphous part of the ceramic exhibits only volume expansion with no microcrystalline stress. Indeed, no microstrains could be detected in the samples. As expected the intensity increase of the broad peak is coupled to an overall decrease of the diffraction peaks.

Iodine-irradiated samples (Fig. 3) also exhibit an increase of amorphous phase with fluence, but starting at lower fluences (as soon as $5 \times 10^{11}$ cm$^{-2}$), thus suggesting a different behaviour of I-irradiation damaging. At intermediate irradiation ($10^{12}$ cm$^{-2}$), again residual strains are present in the sample which unfavour cell parameter determination. In this case, the diagram could still be fitted, however within a poorer reliability, and the cell parameters are determined with larger errors. Interestingly the peak broadening is larger than for Kr-irradiation, mean crystallite sizes being around three times smaller ($\approx 100$ nm). The iodine irradiation creates more crystalline perturbation. Looking at small angles for low fluence (Fig. 3(a)), one can see some discrepancies in peak positions with the refined parameters. This may also be the sign of residual strains present in a partially elastically deformed material, with the simultaneous presence of plastic zones corresponding to the amorphous volume.

From the analysis of the X-ray data, we deduced the amount of crystalline phase remaining after irradiation, cell parameters in the crystalline and microcrystalline phases, their relative and absolute variations as well as their grain sizes. Whatever the ion used for irradiation, a strong increase in amorphous volume with fluence is observed. However, the results of the simulations show a clear difference between both incident ions: with increasing krypton fluence, a steep decrease in

the fraction of crystalline phase is observed between $5 \times 10^{12}$ and $10^{13}$ cm$^{-2}$ (Table 2). Conversely, upon increase in iodine fluence, the decrease in crystalline phase amount is larger than for Kr-irradiation but exhibits a smoother evolution.

After a strong increase of the unit-cell with irradiation, for the highest doses, the unit-cell parameters of the crystalline phase are approximately coming back to their starting, non-irradiated values. Simultaneously, we do not observe any significant change in the mean crystallite size. The increase in amorphous phase fraction is then associated to the unit-cell expansion up to a value for which the whole material relaxes into unstrained crystalline and amorphous phases. The elastic deformation increase of the crystalline phase up to the $10^{13}$ cm$^{-2}$ fluence is fully relaxed for $5 \times 10^{13}$ cm$^{-2}$ in the case of Kr irradiation. Such a process alone would tend to a progressive complete amorphization of the material with decreasing crystallite sizes due to damage. However this is not observed, and the amorphized fraction gets saturated around 85% of the material. This is a good indication that another phenomenon competes with the amorphization process. Heat exchanges are probably large during irradiation, which may promote recrystallisation and at least would explain the conservation of the mean crystallite sizes.

Variations of the damaged fraction in the material $F_d$ ($F_d = 1 - F_c$ with $F_c = V_c/V$) are plotted versus fluence on a linear scale (Figs. 4(a) and (b)): the damaged fraction in I-irradiated fluorapatite sinters can be fitted properly with the classical Poisson's relation $F_d = B[1 - \exp(-A\Phi t)]$ where the cross section for amorphization $A$ is defined as $A = \pi R^2$ and $B$ is a maximum value of amorphization characteristic of fluoroapatite. A second order relation $F_d = B[1 - (1 + A\Phi t) \exp(-A\Phi t)]$ was also used to fit experimental data in the case of Kr irradiated samples. The latter relationship implies a double impact model for the damage creation. This kind of relation was already used by Gibert-Mougel and coworkers [19] and Benyagoub [20] to account for the phase transformation of zirconia, from monoclinic to tetragonal symmetry, upon heavy ion irradiations. The results of the
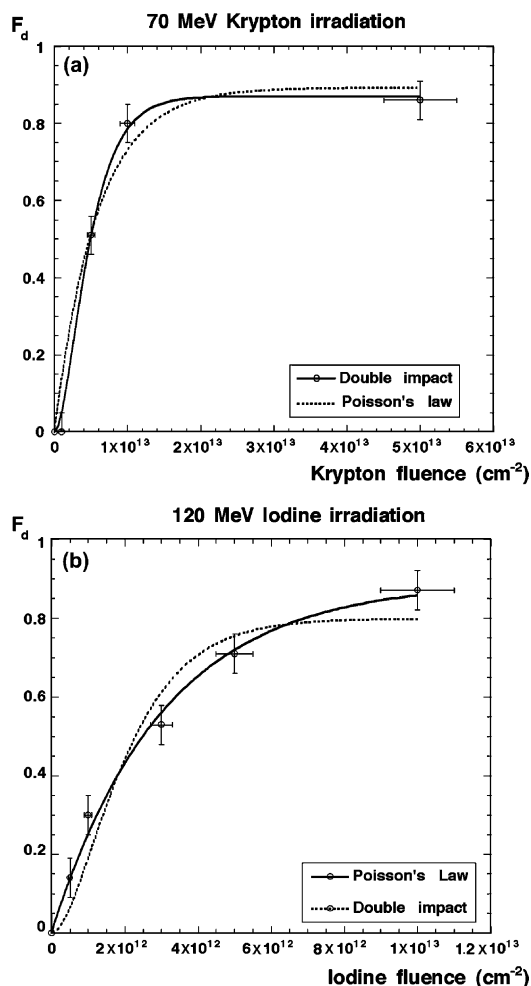
Fig. 4. Best fits of the damage curves using single and double impact models for (a) 70 MeV krypton irradiation and (b) single and double impact for 120 MeV iodine irradiation.

fits are presented in Table 3: the $\chi^2$ values show that a double impact model fits better the Kr data whereas a single impact can be used properly for iodine irradiation. Consequently amorphous track core diameters are found to be constant within experimental errors after Kr double impact and iodine single impact. Moreover in both cases, B values, which correspond to the maximum amorphization rate that can be obtained in fluorapatite for a given electronic energy loss, increase from Kr ($\approx 85\%$) to iodine ($\approx 90\%$) irradiation in agreement with the increase of the electronic stop-

ping power. The fact that a complete amorphization of fluorapatite cannot be obtained even for high fluences, confirms the defect healing behaviour of this material already quoted by Soulet and coworkers [10] upon α irradiation (Table 4).

Owing to previous electron microscopy observations [17], latent tracks formed in the wake of krypton ions in the electron energy loss regime must present an amorphous core which accounts for the amorphization of the fluorapatite through their overlapping. But it was also shown that the existence of amorphous material in the track core depends on the track size and morphology [26]: for small track ($R \leqslant 2 \, nm$), like the one shown in Fig. 1, tracks are composed of bubbles of defects extending along the ion path, in which the presence of amorphous matter could never be proved. Thus it is likely that, at low krypton fluence, where no overlapping of ion tracks occurs, one observes small bubbles of extended defects and that a second impact, at higher fluence, is necessary to create amorphization.

Table 2 also reveals an expansion of the cell parameters upon increase in the Kr fluence up to $10^{13} \, cm^{-2}$. Above this fluence, for $5 \times 10^{13} \, cm^{-2}$, the cell parameters show a decrease and tend to recover the initial value. The latter result may be due to a partial annealing of defects above a fluence of $10^{13} \, cm^{-2}$, annealing which induces a saturation in the damage around 85% of amorphous phase. Annealing of some defects results in a relaxation of stress on the remaining crystallized zones which thus recover the initial apatitic structural parameters. For iodine irradiation, variations of the crystalline fraction $F_c$ parameters can be observed (Table 2) although smaller than after Kr irradiation. This could be related to the difference in the damage creation mechanism between I and Kr irradiations mentioned above: a single iodine impact would allow creation of an amorphous core in latent tracks whereas a double Kr impact would be necessary to amorphize the fluorapatite giving rise, after a single impact, to small domains of damage mainly built of stressed matter.

In both cases, the striking result of this study is the absence of total amorphization of fluorapatites upon swift heavy ion irradiation: $F_d^{max}$ ranges between 80% and 90%, depending on the model used

Table 3
Results of the fits of fluorapatites damage curves using single and double impact models as shown in Figs. 4(a) and (b)

| Fitting parameters | Krypton | | Iodine | |
| --- | --- | --- | --- | --- |
| | Single impact $F_d =$ $B(1-\exp(-A\phi t))$ | Double impact $F_d =$ $B(1-(1 + A\phi t)\exp(-A\phi t))$ | Single impact $F_d =$ $B(1-\exp(-A\phi t))$ | Double impact $F_d =$ $B(1-(1 + A\phi t)\exp(-A\phi t))$ |
| $A = \pi R^2$ (cm$^2$) | $1.71 \pm 0.15 \times 10^{-13}$ | $3.9 \pm 0.15 \times 10^{-13}$ | $3.3 \pm 0.15 \times 10^{-13}$ | $9.5 \pm 0.15 \times 10^{-13}$ |
| Radius $R$ (nm) | $2.3 \pm 0.2$ | $3.5 \pm 0.2$ | $3.2 \pm 0.3$ | $5.4 \pm 0.3$ |
| $B$ (max. damage rate) | $0.87 \pm 0.2$ | $0.85 \pm 0.2$ | $0.9 \pm 0.2$ | $0.80 \pm 0.2$ |
| $\chi^2$ | 0.025 | 0.003 | 0.003 | 0.032 |

Table 4
Variations of peak positions with fluence at the [0 0 2] reflection of single crystals of fluorapatite as seen on X-ray diffractograms shown in Figs. 5 and 6

| | Fluence (ions cm$^{-2}$) | Virgin | | Stressed | | |
| --- | --- | --- | --- | --- | --- | --- |
| | | Angular position | $c$ | Angular position | $c$ | $\Delta c/c_0$ |
| Pristine | 0 | 25.871(2) | 6.8821(2) | – | – | – |
| Kr irradiated | $10^{11}$ | | | 25.858(2) | 6.8855(2) | 0.0494 |
| | $10^{12}$ | 25.868(2) | 6.8829(2) | 25.617(2) | 6.9492(2) | 0.9750 |
| | $5 \times 10^{12}$ | 25.868(2) | 6.8829(2) | – | – | – |
| | $10^{13}$ | 25.869(2) | 6.8826(2) | – | – | – |
| | $5 \times 10^{13}$ | 25.871(2) | 6.8821(2) | – | – | – |
| I irradiated | $10^{11}$ | | | 25.843(2) | 6.8894(2) | 0.1060 |
| | $5 \times 10^{11}$ | 25.874(2) | 6.8813(2) | 25.734(2) | 6.9181(2) | 0.5230 |
| | $10^{12}$ | 25.877(2) | 6.8806(2) | 25.586(2) | 6.9575(2) | 1.0956 |
| | $3 \times 10^{12}$ | 25.879(2) | 6.8800(2) | – | – | – |
| | $5 \times 10^{12}$ | 25.880(2) | 6.8798(2) | – | – | – |
| | $10^{13}$ | 25.874(2) | 6.8813(2) | – | – | – |

for simulation, for Kr and I irradiations. Thus it appears that this material is submitted to a competitive process between amorphization and crystallization depending on the $(dE/dx)_e$ value.

In the case of carbon irradiation, for which the electron energy loss lies below the threshold for creation of latent tracks (5 keV/nm) [21], no amorphous phase could be detected by powder X-ray diffraction up to a fluence of $10^{15}$ cm$^{-2}$.

### 3.2. Fluorapatite single crystals

X-ray diffraction on single crystals of fluoroapatite was used to investigate the stress induced by heavy ion irradiation. Only the [0 0 2] reflection was used in a first step giving only access to the $c$ parameter of the structure. The mean free path of the 7979 eV X-ray photons was estimated to

37 μm from the absorption constants of the elements, thus much larger than the calculated I, Kr and C projected ranges.

The $\theta$–$2\theta$ diffractograms for the krypton irradiated single crystals are shown in Fig. 5. The pristine sample diffractogram exhibits one peak at 25.871(2)° corresponding to $d_{0 0 2} = 3.4410(3)$ Å. As shown in Table 1, 70 MeV krypton ions start depositing an energy on the electrons of the target of 12.7 keV/nm at the surface decreasing very quickly inside the 9.4 μm thickness of the irradiated layer. At a depth of 1 μm from the range of the krypton ions, the energy loss starts to be mainly due to nuclear collisions such that the irradiated layer must be seen as a composite between 8 μm of damage induced by electronic energy loss and 1.4 μm of damage mainly created by cascades of nuclear collisions.
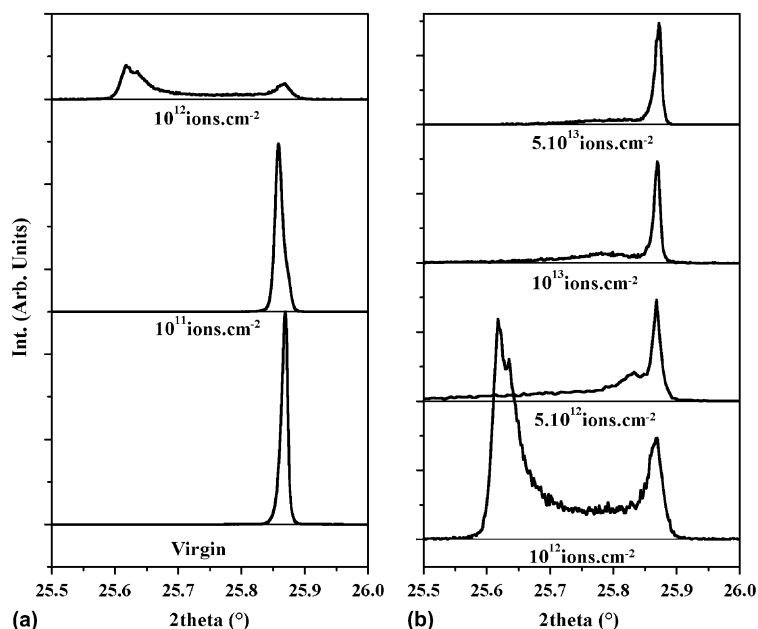
Fig. 5. (001) single crystal diffraction scans around the (002) line for Kr-irradiated samples. (a) Lower fluences with normalized integrated intensity. (b) Larger fluences with normalized non distorted (002) peak intensity (see text).

Upon increasing krypton fluence, the [002] reflection is split into two peaks: one keeps exactly the same angular position, whatever the analysed sample; and is correlated to the remaining virgin material below the damaged layer. The second one is shifted toward low angles by more than $0.2°$ for $10^{12}$ cm$^{-2}$, indicating that the $c$ parameter of the irradiated material has expanded by about 1%. This second peak keeps a small width, which outlines a large coherence length and a homogeneous distribution of the corresponding $c$ parameter in large parts of the irradiated layer. The observed shift is due to the stress induced by the latent tracks in the surrounding material of the irradiated layer. This stress is created by the volume expansion of the track core and is relaxed through an expansion parallel to the $c$-axis since any lateral expansion is blocked by the pristine single crystal lying below. Such a result was already observed in heavy ion irradiated thin film of magnetic oxides (YIG, hexaferrite) [22–27] where the thin film is linked to the substrate on which it is deposited. Between the two peaks, one can observe a plateau corresponding to a continuous transition between

strained and relaxed zones of the crystal and so, to inhomogeneous distribution of $c$ parameters between the two extreme values. These observations do not allow us to discriminate which parts of the samples are characterized by such intermediate stresses, but owing to the penetration depth of the X-ray beam, one can assume their origin to be the final damaged layer before the deep pristine apatite. For these smaller fluences, the fraction of amorphized volume can be neglected and the corresponding curves in Fig. 5(a) have their integral intensity normalized.

Similar results can be observed at small fluences for fluorapatite single crystals irradiated by 120 MeV Iodine ions (Fig. 6) exhibiting a slightly larger thickness range of perturbation than krypton ions ($R_p \approx 12.7 \mu m$). From $10^{11}$ to $10^{12}$ I cm$^{-2}$, an intense peak appears shifted toward low diffraction angles with respect to the initial position of the [002] reflection, the shift increasing with the fluence up to $10^{12}$ I cm$^{-2}$ and reaching the same maximum value as for krypton irradiation at the same fluence (Figs. 5 and 6). As the damaged thickness range of iodine is larger than for Kr ions,
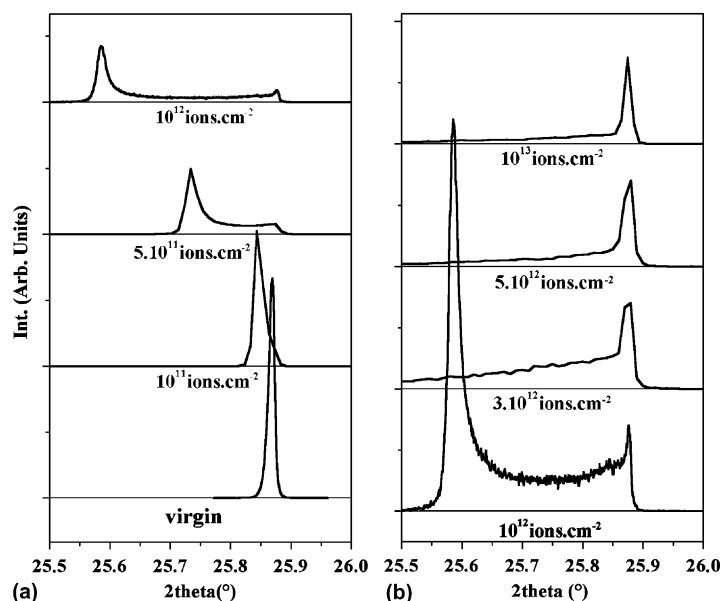
Fig. 6. (0 0 1) single crystal diffraction scans around the (0 0 2) line for I-irradiated samples. (a) Lower fluences with normalized integrated intensity. (b) Larger fluences with normalized non distorted (0 0 2) peak intensity (see text).

the shifted peak is relatively more intense in comparison with the residual peak of the deep pristine apatite. The continuous shift of the strain is clearly visible between $10^{11}$ and $10^{12}$ I cm$^{-2}$ fluences (Fig. 6).

The relative variation of the *c* parameter seems here twice as large as the refined values in the ceramic samples for the largest fluence analysed in single crystals. This can be due to at least two phenomena. Firstly, the specific orientation of the irradiation along the *c* axis in the case of the single crystal experiments, in comparison with the more random one in the case of the sinters. Any anisotropic damage which would be favoured along a specific crystallographic direction, i.e. *c*-axes as in this work, is somehow averaged over all the orientations of the crystallites in the ceramics. Secondly, the much larger resolution of the instrument used for the single-crystal experiments makes the separation of the two diffracting components (virgin and damaged) available, which is not the case using the powder diffraction instrument. The parameter variations are consequently observed in the latter case as a mean value among the component contributions.

For increasing Kr- and I-fluences above $10^{12}$ cm$^{-2}$, the damage-related peak disappears leaving a diagram with only the peak from virgin material, coming from both the crystal deeper than the irradiated layer and relaxed or recrystallised parts of the crystals, and a broad contribution at slightly smaller angles due to some distribution of remaining stresses inside the irradiated layer. In this case, the amorphization rate becomes important and must result in a decrease of the global integrated intensity. But, one can make the assumption that the contribution of the undistorted part of the sample below the damaged layer should be constant and it is the reason why the curves in Fig. 5(b) and Fig. 6(b) have been normalized by the corresponding maximum peak intensity. For fluences between $10^{12}$ and $5 \times 10^{12}$ ions cm$^{-2}$, one still observes a very large plateau with larger *c* parameter values. This result is coherent with the powder X-ray diffraction results which showed a sharp increase of the volume of amorphized material. Above $10^{12}$ ions cm$^{-2}$, the intensity corresponding to the extended part of the damaged layer abruptly falls down, but one still observes a significant contribution to the diffracted

intensity at lower angles. Such a sudden disappearance, above $10^{12}$ ions cm$^{-2}$ of the shifted peak, attributed to the stressed domains around the track cores, can be explained by the track overlap at high fluence which relieves most of the stressed domain. The broad distribution of the low angle contributions, clearly visible on diffractograms for fluences ranging from $3 \times 10^{12}$ I cm$^{-2}$ to $5 \times 10^{12}$ Kr cm$^{-2}$, could be understood as to be due either to some small stress in the residual crystallized material or/and to stress induced in the ion stopping zone around the cascades of nuclear collisions.

Further X-ray single crystal diffraction investigations are currently performed in grazing incidence to eliminate the contribution of the single crystal below the irradiated layer and for different reflections in order to check the *a* parameter variations and anisotropy.

## 4. Conclusion

Analysis of powder X-ray diffraction patterns of fluoroapatite sinters irradiated with 128 MeV iodine and 70 MeV krypton ions showed that different irradiation mechanisms are involved in the electronic stopping power regime. With iodine irradiation, the amorphized fraction of the material could be easily fitted using the classical Poisson's law showing that latent tracks exhibiting an amorphous core (3.6 nm diameter) are created with a single ion. Conversely, with krypton irradiation, variations of the amorphized fraction versus fluence seems to follow a double impact process which results in amorphous track cores of the same diameter. The small variation of track diameter upon electronic energy loss is confirmed by TEM observations of Kr irradiated material. Analysis of single crystal X-ray diffractograms, using the [0 0 2] reflection of the fluorapatite structure, shows an expansion of the *c* parameter at low fluence which can be generated by the stress due to the volume increase of the track core as already observed in magnetic oxides. Finally, even at high fluences, a crystallized fraction of 10% still remains showing that complete amorphization of the fluorapatite cannot be achieved. This result confirms the existence of healing process of defects in this material.

## References

[1] W. Weber, R.C. Ewing, C.R.A. Catlow, T. Diaz de la Rubia, L.W. Hobbs, C. Kinoshita, Hj. Matzke, A.T. Motta, M. Nastasi, E.H.K. Salje, E.R. Vance, S.J. Zinkle, J. Mater. Res. 13 (1998) 1434.
[2] R. Erwing, W. Weber, F. Clinard Jr., Prog. Nucl. Energy 29 (1995) 63.
[3] S. Wang, G. Lumpkin, L. Wang, R. Ewing, Nucl. Instr. and Meth. B 166–167 (2000) 293.
[4] M. Beauvy, T. Duverneix, C. Berlanga, R. Mazoyer, C. Duriez, J. Alloys. Compd. 271–273 (1998) 557.
[5] R. Konings, D. Haas, C. R. Phys. 3 (2002) 1013.
[6] T.J. White, D. Zhili, Acta Crystalligr. B 59 (2003) 1.
[7] C. Gaillard et al., Nucl. Instr. and Meth. B 161 (2000) 646.
[8] D. Cherniak, Geochim. Cosmochim. Acta 64 (2000) 3871.
[9] D. Gosset et al., J. Nucl. Mater. 303 (2002) 115.
[10] S. Soulet et al., Nucl. Instr. and Meth. B 132 (1997) 447.
[11] S. Ouchani et al., Nucl. Instr. and Meth. B 132 (1997) 147.
[12] W. Weber et al., J. Nucl. Mater. 250 (1997) 147.
[13] R.A. Young, J.C. Elliot, Archs Oral Biol. 11 (1996) 699.
[14] Balzar, J. Appl. Cryst. 25 (1992) 570.
[15] J. Ricote, D. Chateigner, Boletín de la Sociedad Española de Cerámica y Vidrio 38 (6) (1999) 587.
[16] D. Chateigner, L. Lutterotti, T. Hansen, ILL Highlights 1997 (1998) 28.
[17] L. Lutterotti, S. Matthies, H.-R. Wenk, in: J.A. Szpunar (Ed.), Textures of Materials, Vol. 2, NRC Research Press, Ottawa, 1999, p. 1599.
[18] T.A. Paul, P.G. Fitzgerald, Amer. Miner. 77 (1992) 336.
[19] G. Gibert-Mougel et al., J. Nucl. Mater. 295 (2001) 121.
[20] A. Benyagoub, Nucl. Instr. and Meth. B 206 (2003) 132.
[21] R. Tisserand, M. Rebetez, M. Grivet, S. Bouffard, A. Benyagoub, F. Levesque, J. Carpéna, Nucl. Instr. and Meth. B 215 (2004) 129.
[22] F. Studer, D. Groult, N. Nguyen, M. Toulemonde, Nucl. Instr. and Meth. B 19&20 (1987) 856.
[23] A. Meftah, N. Merrien, N. Nguyen, F. Studer, H. Pascard, M. Toulemonde, Nucl. Instr. and Meth. B 59–60 (1991) 605.

[24] F. Studer, Ch. Houpert, D. Groult, J. Yun Fan, A. Meftah, M. Toulemonde, Nucl. Instr. and Meth. B 82 (1993) 91.

[25] M. Toulemonde, S. Bouffard, F. Studer, Nucl. Instr. and Meth. B 91 (1994) 108.

[26] J.-M. Costantini, F. Studer, J.-C. Peuzin, J. Appl. Phys. 90 (1) (2001) 126.

[27] F. Studer, C. Houpert, H. Pascard, R. Spohr, J. Vetter, J. Yun Fan, M. Toulemonde, Radiat. Eff. Def. Sol. 116 (1991) 59.